Tollmien-schlichting waves over forward-facing steps
an experimental and numerical study

Barahona, M.; Rius-Vidales, A. F.; Tocci, F.; Ziegler, P.; Hein, S.; Kotsonis, M.

Publication date
2022

Document Version
Final published version

Citation (APA)
Barahona, M., Rius-Vidales, A. F., Tocci, F., Ziegler, P., Hein, S., & Kotsonis, M. (2022). *Tollmien-schlichting waves over forward-facing steps: an experimental and numerical study*. Paper presented at 12th International Symposium on Turbulence and Shear Flow Phenomena, TSFP 2022, Osaka, Virtual, Japan.

Important note
To cite this publication, please use the final published version (if applicable).
Please check the document version above.

12th International Symposium on Turbulence and Shear Flow Phenomena (TSFP12)
Osaka, Japan (Online), July 19-22, 2022

TOLLMIEN-SCHLICHTING WAVES OVER FORWARD-FACING STEPS: AN EXPERIMENTAL AND NUMERICAL STUDY

M. Barahona[1*], **A. F. Rius-Vidales**[1*], **F. Tocci**[2], **P. Ziegler**[3], **S. Hein**[2] **and M. Kotsonis**[1]
1: Section of Aerodynamics, Delft University of Technology, Delft, The Netherlands.
2: Institute of Aerodynamics and Flow Technology, German Aerospace Center (DLR), Göttingen, Germany.
3: University of Stuttgart, Stuttgart, Germany.
*Correspondent authors: m.barahonalopez@student.tudelft.nl and a.f.riusvidales@tudelft.nl

ABSTRACT

This work presents an experimental and numerical investigation jointly conducted by TU Delft and DLR on Tollmien-Schlichting (TS) waves interaction with a Forward-Facing Step (FFS). Experiments are conducted at the TU Delft low-turbulence anechoic wind tunnel on an unswept flat plate model. Single-frequency disturbances are introduced using controlled acoustic excitation. The temporal response of the flow in the vicinity of the step is measured using Hot-Wire Anemometry (HWA). In addition, the global effect of the step on laminar-turbulent transition is captured using Infrared Thermography (IR). Two-dimensional (2-D) Direct Numerical Simulations (DNS) performed at DLR provide detailed information at the step. Experimental and DNS results in clean and step case conditions present very good agreement. Both methods predict large distortion of the TS waves downstream of the step, where DNS results present different growth trends between $|\hat{u}|$ and $|\hat{v}|$ components of the TS waves. Furthermore, negative and positive regions of the production term are observed to correlate with streamwise positions where the disturbances appear tilted in and against the mean shear, respectively. These findings point towards the presence of different growth mechanisms triggered by the step which could modify the level of amplification of disturbances far downstream.

INTRODUCTION

The presence of panel discontinuities on aircraft wings can lead to laminar-turbulent transition advancement and an increase in skin-friction drag. The recent interest in low-speed aircraft for regional air mobility has drawn attention to the effect of surface irregularities on unswept wings, where transition is dominated by Tollmien-Schlichting (TS) waves. Panel discontinuities are commonly modeled in the form of two-dimensional steps. Prior subsonic studies in TS dominated transition have shown that a Backward-Facing Step (BFS) configuration is more detrimental than a Forward-Facing Step (FFS) (Wang & Gaster, 2005; Crouch *et al.*, 2006). Therefore, in the design of laminar flow components, FFSs are preferred over BFSs.

First research efforts concerning FFS-induced transition aimed at finding critical Reynolds heights (e.g. $\mathrm{Re}_{h,\mathrm{crit}}$) to provide manufacturers with a rapid estimate of the transition location and the maximum permissible height between panel discontinuities. However, it was soon proven from the experiments of the Northrop Grumman Corporation (Drake *et al.*, 2010) that the large dependency of the transition location on the specific test conditions makes $\mathrm{Re}_{h,\mathrm{crit}}$ alone not sufficient to determine when FFSs become critical.

The experimental results of Wang & Gaster (2005) suggested that transition with FFS could be largely described by the exponential growth of disturbances downstream. Their results were in agreement with observations from other authors, whose focus was on developing a semi-empirical model inspired on the e^N-method to predict transition location (Perraud *et al.*, 2004; Crouch *et al.*, 2006). These models attempt to isolate the effect that the step has on transition in one single parameter, ΔN. Large discrepancies are observed when the data fits and models proposed by different authors are compared, as noticed in (Costantini, 2016). The outcomes of the aforementioned studies raise the question of whether the effect of an FFS on transition can be uniquely described by ΔN.

Recent DNS and experiments in 3D boundary layers dominated by Crossflow Instabilities (CFI) in the presence of FFS point to different growth mechanisms at the step. These could explain the observed delay on transition for some step heights (Rius-Vidales & Kotsonis, 2021), the unsteadiness of the shear layer downstream (Eppink, 2020) or the onset of near-wall vortices immediately after the step (Casacuberta *et al.*, 2021). Despite the different incoming instability in these works, compared to TS waves, their findings emphasize the importance of close-examining the disturbances evolution in the vicinity of a FFS to understand how this could influence transition downstream.

From the aforementioned works the mechanisms governing the growth of disturbances at the step remain not fully understood. In turn, the lack of comparison between numerical and experimental data further hinders the problem understanding. On the one hand, existing experimental works on TS-FFS dominated transition were mainly concerned with transition prediction, providing limited measurements in the vicinity of the step. On the other hand, previous numerical studies were not designed to match other experimental works. In light of this, the aim of this study is to close-examine the TS waves at the step to identify which are the relevant mechanisms that modify their growth and move transition upstream.

EXPERIMENTAL SET-UP

The experiments were performed in the A-tunnel, an open-jet, closed-circuit, subsonic, vertical wind tunnel. The anechoic test chamber features acoustic absorbing foam which reduces sound reflections. This creates a suitable environment to force and study TS waves since these are highly responsive

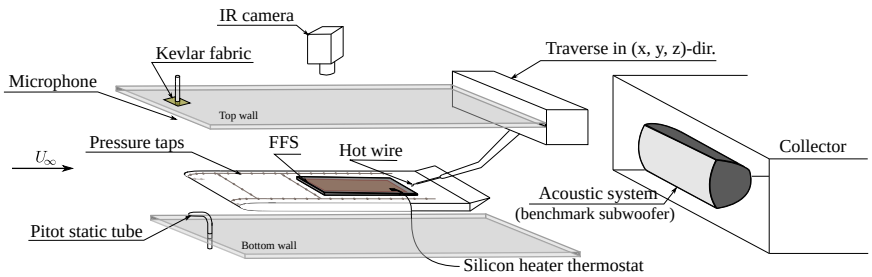

Figure 1: Experimental set-up. Schematic showing the FFS location, the acoustic unit and the different measurement techniques used.

to acoustic emissions. A nozzle is used to adapt the circular inlet test section of diameter 600 mm to a rectangular one with dimensions 500× 500 mm^2 containing an unswept flat plate model with a chord of $c = 950$ mm at zero angle-of-attack. The flat plate features a Modified Super Ellipse (MSE) at the leading edge (LE) with aspect ratio AR = 6. This design moves the suction peak towards the LE and reduces the adverse pressure gradient in the LE region (Lin *et al.*, 1992), ensuring a rapid development towards a Blasius boundary layer. The stagnation point and the LE pressure distribution can be adjusted with a trailing edge (TE) flap. The flow on the bottom side is forced to turbulence using a zig-zag tape to avoid uncontrolled shedding. The external velocity over the measurement side is set to $U_{\text{ref}} = 22.5$ m/s which results in a Reynolds number based on the chord of $\text{Re}_c = 1.32 \times 10^6$ and a freestream turbulence intensity below 0.1% (bandwidth $5 - 2 \times 10^5$ Hz). Finally, adjustable FFSs at $x/c = 0.4$ are created using a built-in mechanism (see Figure 1). The step heights are characterized by traversing a Micro-Epsilon 3010-25BL laser scanner (resolution of 1.5 μm) along the span. The step is located at $x_h = 380$ mm.

Single-frequency TS waves are excited using acoustic forcing. A 120W benchmark subwoofer located 2.15 m downstream of the LE is used to generate a continuous acoustic signal at the forcing frequency of interest. The model's MSE LE removes the curvature discontinuity between the flat plate and LE juncture, ensuring receptivity only at the nose of the LE (Lin *et al.*, 1992). The acoustic wave amplitude and frequency are monitored using a GRAS 46BE analog free-field microphone flushed-mounted close to the LE. In addition, Kevlar type 120 fabric covers the side of the microphone facing the flow to reduce the permeability to hydrodynamic fluctuations with respect to sound waves. In these conditions, the signal-to-noise ratio (SNR) was always higher than 10.

Fifteen boundary layer profiles were measured using Hot-Wire Anemometry (HWA) along the model's midspan (the measurement region covers 40 mm upstream and 40 mm downstream of the step) with a single-wire probe (Dantec Dynamics 55P15). The HWA sampling frequency was set to 51.2 kHz with a total measuring time per point of 3 seconds to ensure statistical convergence. The distance from the last HWA point to the wall was measured using a Taylor-Hobson microalignment telescope. In addition, during the post-processing the wall distance was refined using velocity profiles from the DNS. Finally, the amplitude of the forced TS wave is acquired from the Fast-Fourier Transformed (FFT) HWA signal at the excitation frequency.

A silicon heater, electronically controlled by a thermostat, actively heats[1] a portion of the flat plate surface downstream of the step, with dimensions of 500×300 mm. An Optris PI640 camera (640×480 pixels of optical resolution and a thermal sensitivity of 75 mK) equipped with a wide-angle lens ($f = 10.5$ mm) is used to capture the temperature changes across the black acrylic plate (surface emissivity of 0.95) constituting the step. For each measurement 100 frames are recorded at a frequency rate of 3.5 Hz at two different Reynolds numbers to perform Differential Infrared Thermography (DIT). This technique has already proved to be succesful to increase the SNR of the transition front identification (Rius-Vidales & Kotsonis, 2021).

DIRECT NUMERICAL SIMULATIONS

Direct Numerical Simulations (DNS) are performed at DLR using the Nek5000 code by Fischer *et al.* (2008) which is based on the Spectral Element Method (SEM). The SEM decomposes the physical domain into (spectral) elements where the flow field solution is given by a sum of Lagrange interpolants defined by an orthogonal basis of Legendre polynomials up to degree P within each element. The results presented here were obtained with a polynomial order $P = 9$ within the spectral elements.

A boundary layer code developed at the Aerodynamics section in TU Delft is initially used to compute a reference solution for the clean case based on the measured pressure distribution. This solution is used to obtain the boundary conditions imposed in the DNS, allowing to reproduce the experimental conditions, see Table 1.

The DNS investigations focus on the beginning of the transition process and therefore are limited to 2-D domains to reduce the computational costs. The calculations consisted of a DNS of the steady laminar 2-D base flow and succeeding unsteady DNS for the disturbances propagation. For the latter, a harmonic blowing and suction strip centered at $x = 200$ mm is applied at the wall to introduce periodic TS waves. The blowing and suction strip introduces a wall-normal velocity component at a selected frequency with zero net-mass flow. Its amplitude is prescribed such that the developing TS wave matches the amplitude measured with HWA at $x = 340$ mm.

RESULTS

The step heights (h) and forcing conditions used for DNS and experiments are indicated in Table 1. A comprehensive parametric study is performed by means of IR measurements for seven different steps at two forcing frequencies and no forcing. HWA and DNS results will focus on one step case. The forcing frequency of $F = 90$ constitutes a TS mode with highest amplitude at the step region while $F = 110$ undergoes decay at the step.

[1]The surface temperature difference was kept below half a degree to avoid interfering with the transition process.

Table 1: Experimental test cases. Step located at $x/c = 0.4$ and step height spanwise non-uniformity, $\overline{\sigma_h} = 7\ \mu$m. All cases were also run without acoustic forcing. F denotes reduced frequency, $F = \left(2\pi f \nu / U_{\text{ref}}^2\right) \times 10^{-6}$, and δ^* is the displacement thickness in no-step case at $x/c = 0.4$.

(h/δ^*)	$[-0.008^{\dagger}, 0.775^{\dagger}, 1.075, 1.261, 1.462^{\ddagger}, 1.654, 1.950^{\ddagger}]$
$\overline{h}$, μm	$[-8, 732, 1014, 1190, 1380, 1561, 1840]$
F	$[90, 110]$

†: cases measured with HWA and computed with 2D-DNS.

‡: cases measured with HWA.

Transition Front Movement with Step Height

The transition location is defined in this work as the intersection between the model's centerline and a linear fit to the front identified from DIT images (Rius-Vidales & Kotsonis, 2021). Figure 2 (a) shows the Reynolds number based on the transition location ($\text{Re}_{x_T} = x_T U_{\text{ref}}/\nu_\infty$) obtained in the present experiments. In addition, the experimental data from Wang & Gaster (2005) is included given the similarities of their set-up and freestream conditions with the present experiments. In turn, in Wang & Gaster (2005) experiments transition is driven by the model's receptivity to background disturbances while in this work also forced conditions are addressed.

Large differences are observed between the Re_{x_T} values of Wang & Gaster (2005) and this work. There are two plausible reasons for which the transition location in clean case conditions takes place farther upstream in these experiments compared to the ones of Wang & Gaster (2005). First, the turbulent wedges of the test section side-walls could be interferring with the *natural* transition front, promoting early transition. Secondly, receptivity at the LE could be affected by other acoustic sources coming from resonance effects in the open-jet facility, e.g. standing waves (sec. 16.1.4 in Tropea *et al.* (2007)), or from a global feedback loop generated by vortex shedding at the TE.

In FFS-TS transition related literature, ΔN is used to isolate the effect of the step on transition from the freestream conditions, enabling proper comparison between different experimental works. This parameter represents the decrease of the N-factor at transition with respect to the clean case N-factor due to the presence of a roughness element, i.e. $\Delta N = N_{T_0} - N$. The clean transition front takes place outside of the heating plate in these experiments (see Figure 1). Hence, N_{T_0} is instead computed using the N-factor (from linear stability theory) obtained at a higher Reynolds number, for which transition location could be measured.

Figure 2 (b) shows the ΔN results from this work compared to the different models and fits for ΔN from Wang & Gaster (2005), Crouch *et al.* (2006) and Costantini (2016). The present results show a nearly linear dependence of ΔN with the relative step height (h/δ^*), similar to the model proposed by Crouch *et al.* (2006) but with a lower slope, i.e. the FFS appears more detrimental for laminar-turbulent transition in Crouch *et al.* (2006) experiments.

From Figure 2 (b) it can be observed that neither of the models presented nor the present experiment results present good correlation. For instance, while the model of Crouch *et al.* (2006) predicts a gradual movement of the transition front with h/δ^*, the data fit of Wang & Gaster (2005) depicts an exponential-like increase of ΔN, indicating that higher steps quickly advance transition towards the step location compared to smaller steps. Other authors (Edelmann, 2014; Costantini, 2016) have already noticed the large differences on ΔN from different experimental works. Costantini (2016) argued that possible explanations for this could comprise the different measurement techniques used to identify transition location or the effect of the step location. The latter was shown to have almost no effect on ΔN in Crouch & Kosorygin (2020). These results indicate that there appears to be no universal criteria to represent FFS-transition based on a single step or transition parameter. Instead, the effect of the step seems to largely depend on the specific test conditions or transition detection techniques used in each experiment.

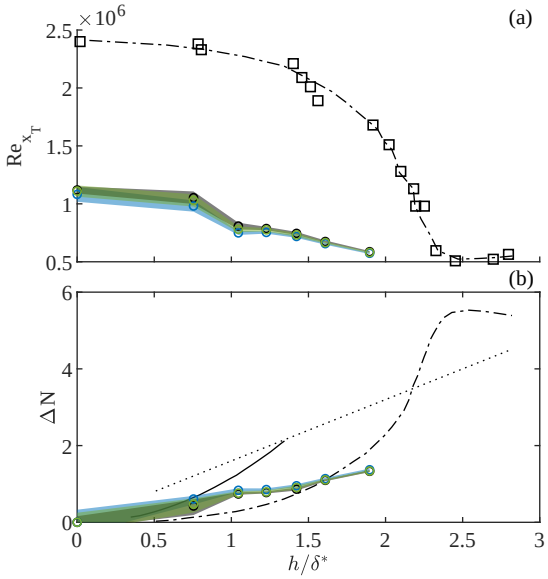

Figure 2: (a) Reynolds transition (Re_{x_T}) as a function of the relative step height (h/δ^*). Data digitized from Fig. 4 in Wang & Gaster (2005) (□) and these experiments (○). (b) N-factor decrease at transition, ΔN, as a function of the relative step height. Data fit digitized from Fig. 7 in Wang & Gaster (2005) (-·-·), Fig. 6.4.2.1 (d) in Costantini (2016) (——), $\Delta N = 1.6 h/\delta^*$ model from Crouch *et al.* (2006) (·····) and the present experiments (○). Unforced (black) and forced conditions at $F = 90$ (blue) and $F = 110$ (green). Shaded regions indicate confidence bands.

Meanflow Modulation at the Step

Figure 3 (a) shows the pressure coefficient at the wall from DNS results. The pressure imposed in the DNS at the top boundary condition is set to match the pressure developing at the wall during experiments in no-step conditions. However, since the pressure exhibits a weak variation in wall-normal direction ($\partial p/\partial y \approx 0$), small differences are observed in Figure 3 (a) when comparing pressure tap measurements and wall pressure from DNS for $h/\delta^* = 0$. Wall pressure in step conditions could not be measured during the experiments since the available pressure taps were located outside the step region (see Figure 1).

The boundary layer is subject to a progressively growing adverse pressure gradient as it approaches the step (Figure 3 (a)). Regions of low momentum close to the wall are subject to large curvature ($\partial^2 U/\partial y^2$) changes due to the pressure gradient. This creates an inflection point within the boundary layer which moves away from the wall as the adverse pressure gradient increases (note contour lines representing the inflection points in Figure 5). The loss of streamwise momentum

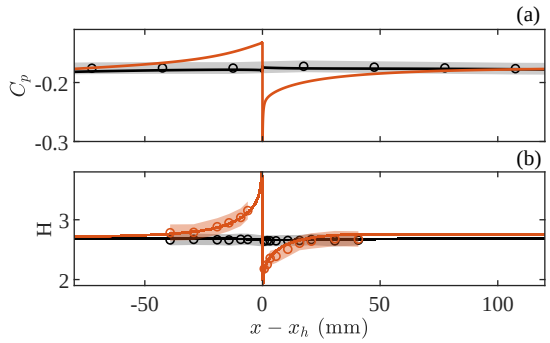

Figure 3: (a) Pressure coefficient at the wall. (b) Shape factor computed from DNS and HWA boundary layer profiles in clean case (black) and step (orange) conditions. Symbols denote experimental data and full lines DNS. Confidence bands for experimental data are included for step (orange) and no-step (black) cases.

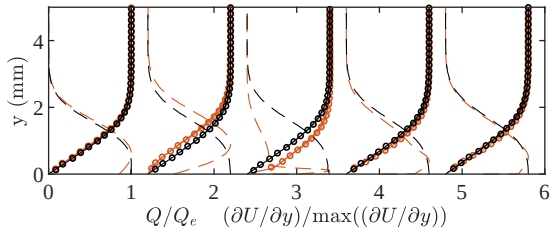

Figure 4: Normalized boundary layer profiles ($Q = \sqrt{U^2+V^2}$) in clean (black) and step (orange) conditions from HWA measurements (○) and DNS results (——) at $x - x_h = [-40, -7, 1, 20, 40]$ mm. Profiles of $\partial Q/\partial y$ are shown in dashed lines. Experimental uncertainty is within symbol size.

close to the wall, forces the boundary layer to expand in y, increasing its shape factor, as observed in Figure 3 (b).

At the step, a strong favorable pressure gradient takes place that is immediately followed by a gradually decreasing adverse pressure gradient downstream. Similar to the experiments of Eppink (2020) with CFI, a kink in U is observed a the step edge concurrent with the explosive growth in V (Figure 5). Figure 3 (b) shows that the shape factor of the boundary layer suddenly drops as a consequence of the strong favorable pressure gradient but smoothly recovers to clean case values downstream. Velocity profiles in Figure 4 provide further insight into the modulation undergone as a consequence of the sudden jump in pressure. After the step the boundary layer presents a dual structure characterized by two different maxima in $\partial U/\partial y$ (also observed from inflection contour lines in Figure 5 (a)). This modular composition of the boundary layer is the result of the curvature change undergone due to the presence of two quasi-simultaneous opposite pressure gradients. It would appear that the effect of such a strong and delimited favorable pressure gradient persists after the step imprinted in the boundary layer curvature. Further downstream this is supressed and the adverse pressure gradient prevails, note the merging of the two $\partial U/\partial y$ peaks from Figure 4 and Figure 5 (a).

Growth of Tollmien-Schlicthing Waves

Figure 6 shows the growth of two different fundamental modes, $F = 90$ and $F = 110$, in clean and step case conditions. TS wave shape functions at different streamwise locations are shown in Figure 7. Given the existence of additional lobes in the TS shape function (observed in both $|\hat{u}|$ and $|\hat{v}|$ components) and the difficulty to distinguish the original TS lobe from the emerging ones, only the TS maxima is tracked to define the N-factor. This explains the abrupt changes in the N-factor curvature observed for $F = 110$ at $x \approx 38$ mm in Figure 6.

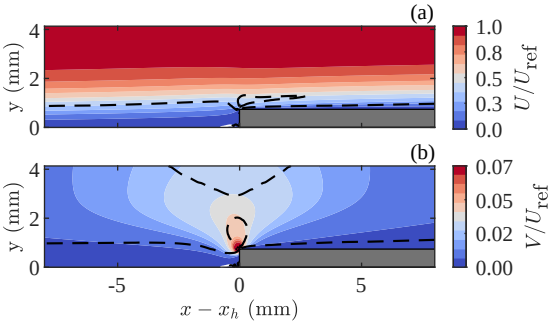

Figure 5: Contours of U (a) and V (b) meanflow components from DNS. Contour lines of $\partial^2 U/\partial y^2 = 0$ in (a) and $\partial^2 V/\partial y^2 = 0$ in (b) are indicated with dashed lines (- - -).

Very good agreement is observed between DNS and experimental results in terms of TS amplification and shape functions from both Figure 6 and Figure 7, respectively. Although experiments do not reach to measure the near-wall peak downstream of the step, they accurately capture the highly distorted TS shape at $x - x_h = 40$ mm, which, interestingly, takes place in a region where the meanflow has already recovered to clean case conditions (see Figure 3 (b)).

Upstream of the step the fundamental mode grows exponentially (Figure 6). It is observed from Figure 7 that the TS wave becomes thicker in regions where the shear stress is maximum upstream of the step. In front of the step, $|\hat{u}|$ decays while $|\hat{v}|$ rapidly increases due to the distortion prompted by the step geometry (Figure 6). After the step edge, a small peak emerges near the wall in $|\hat{u}|$ and $|\hat{v}|$ which coincides with the near-wall peak observed in $\partial U/\partial y$ (see Figure 7). Phase contours (not presented here) show in this region a feature with opposite phase to the incoming TS wave. Zoomed streamlines and vorticity contours in Figure 8 further evince the presence of a vortical structure counterrotating the TS wave on top. Note that this near-wall vortex emerges in regions where no recirculating flow is predicted from DNS. When the near-wall peak amplitude is tracked (not shown here), it is observed to decay in streamwise direction, indicating that the existing TS wave prevails downstream (Figure 8). Within this region the TS wave undergoes a pronounced stabilization (Figure 6). Further downstream the fundamental mode keeps on stabilizing more gradually up to $x - x_h = 40$ mm, where it starts to destabilize again. Interestingly, all higher harmonics (not shown here) grow significantly just upstream of $x - x_h = 40$ mm, indicating that non-linear effects might become important in the vicinity of this region. However, given their low amplitudes compared to the fundamental mode (20 times larger than the second harmonic), the growth of disturbances remains mainly linear upstream and downstream of the step.

From Figure 6 it can be noticed that the growth of the fundamental mode becomes highly complex downstream of the step. The appearance of several inflection points in the N-factor curve together with the emergence of additional lobes in the shape function constitute some indicators of this. Furthermore, slightly upstream and far downstream of the step $|\hat{u}|$

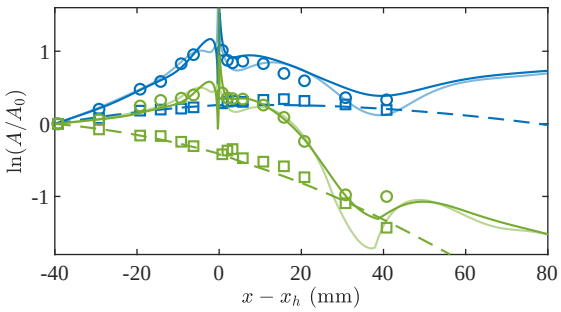

Figure 6: N-factor evolution of the TS wave $|\hat{u}|$ maximum in clean case (- - -) and step conditions (——) for forcing frequencies $F = 90$ (blue) and $F = 110$ (green). Lines denote DNS data and symbols HWA measurements. N-factor based on the maximum of $|\hat{v}|$ is represented by a light-colored line.

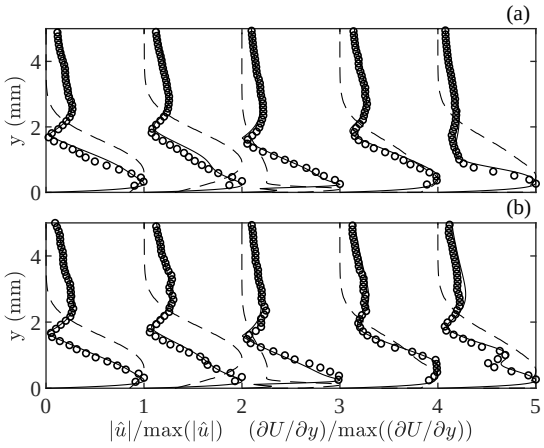

Figure 7: TS shape function at $x - x_h = [-40, -7, 1, 20, 40]$ mm for forcing frequencies $F = 90$ (a) and $F = 110$ (b) in step case conditions. Lines denote DNS data and symbols HWA measurements. Dashed lines correspond to profiles of the mean shear, $\partial U/\partial y$.

and $|\hat{v}|$ maxima exhibit different growth rates, indicating that the growth of TS waves cannot be uniquely described in exponential form in these regions[2].

Figure 9 (a) presents the instantaneous streamlines and $\Re(\hat{u})$ (real part of $\hat{u}$) contour fields downstream of the step at a given phase of the TS cycle to gain insight into the flow features that give rise to the complex growth behavior observed after the step. Examination of the production term is well-suited to analyze the linear growth mechanisms that contribute to stabilize or destabilize the disturbances. The production term from the energy balance of the fundamental mode (see mathematical development in Section C of Jin *et al.* (2021)) is expressed as

$$\hat{\mathcal{P}} = -(\hat{u}_i^* \hat{u}_j + \hat{u}_i \hat{u}_j^*) \frac{\partial U_i}{\partial x_j}, \tag{1}$$

where the superscript * denotes complex conjugate. Figure 9 (b) shows the four different contributions to the production

[2]Similar conclusions are derived when the N-factor is defined as the integral of the different TS shape function components ($|\hat{u}|$ and $|\hat{v}|$) along y, i.e. $\int_0^{h_{\mathrm{DNS}}} |\hat{u}_i|^2 \, dy$

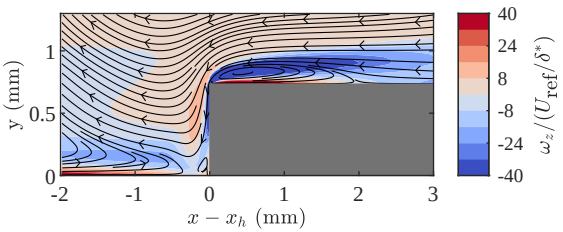

Figure 8: Contours of the normalized spanwise vorticity and disturbance streamlines around the step corner. Forcing frequency $F = 90$ and phase $\phi = \pi$ rad. Wall-normal axis is scaled by 5/3 for visualization purposes.

term and the total value integrated in wall-normal direction, i.e. $\hat{\mathcal{P}} = \int_0^{h_{\mathrm{DNS}}} \hat{\mathcal{P}} dy$ with h_{DNS} being the DNS domain height. From Figure 9 (b) it is observed that the dominant term is $\hat{\mathcal{P}}_{12}$, which can be expressed in terms of the disturbances amplitude and phase:

$$\hat{\mathcal{P}}_{12} = -2\,|\hat{u}|\,|\hat{v}| \cos(\varphi_u - \varphi_v) \frac{\partial U}{\partial y}. \tag{2}$$

This last expression indicates that the increase or decrease on production takes place in regions of high shear where $\hat{u}$ and $\hat{v}$ are not in quadrature, i.e. $(\varphi_u - \varphi_v) \neq \pm\pi/2$.

In overall, it is observed from Figure 9 (a) and (b) that structures tilted against the shear (note stations $-10 \leq x \leq 2$ and $40 \leq x \leq 80$) seem to correlate with regions of positive production where the disturbance is amplified (Figure 6) and viceversa. Interestingly, in a region around $x \approx 35$ mm, production becomes zero, the disturbances achieve very low amplitude and immediately downstream the direction of tilting is changed. Further downstream the TS waves recover its upright position (i.e. $(\varphi_u - \varphi_v) \approx \pm\pi/2$) and production goes back to clean case values.

Based on previous works, the growth of disturbances as a result of their tilting against the shear can be associated to the Orr-mechanism. Åkervik *et al.* (2008) studied the stability of a Blasius boundary layer subject to 2-D disturbances by means of non-modal analysis and observed that the Orr mechanism is the most optimal condition to initiate TS waves. Their results show the evolution of a wavepacket tilted against the shear which effectively amplifies the disturbance linearly until it forms a well-developed TS wave which switches to exponential growth downstream. The authors observe that when only TS type modes are considered, the predicted maximum growth is much lower. Despite the differences with the present results, where the incoming disturbance is already a well-developed TS wave, Åkervik *et al.* (2008) findings manifest the importance of accounting for non-modal growth to correctly evaluate the energy of the disturbance further downstream.

CONCLUSIONS AND FUTURE WORK

The stability of TS waves in the presence of an FFS has been studied by means of experiments and DNS with focus on the growth mechanisms and flow features emerging at the step region. Additionally, the global effect of the step on transition was analyzed from IR measurements. The present results show poor correlation with the existing ΔN models and fits found in literature, which in addition present large differences among the works of different authors. These observations indicate the

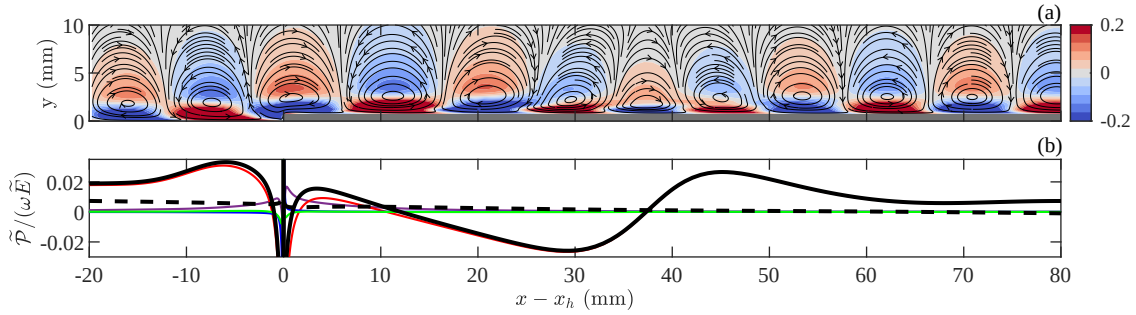

Figure 9: (a) Contours of $\Re(\hat{u})/U_{\text{ref}}$ (%) and streamlines from DNS for the fundamental mode with frequency $F = 90$ at phase $\phi = \pi$ rad. (b) Streamwise evolution of the production term as defined in Equation 1 at reduced frequency $F = 90$. Full lines indicate step case and dashed lines clean case. Different production terms are included in the step case: $\hat{\mathcal{P}}_{11}$ (magenta), $\hat{\mathcal{P}}_{12}$ (red), $\hat{\mathcal{P}}_{22}$ (blue), $\hat{\mathcal{P}}_{21}$ (green) and total production (black). Production is normalized with the disturbance kinetic energy integrated along y, $\tilde{E}$, and the TS frequency, $\omega = 2\pi f$.

difficulty of describing the effect of an FFS on transition with a few non-dimensional parameters.

Meanflow quantities, N-factors and shape functions of the fundamental mode from 2D-DNS and experiments show very good agreement for two different forcing frequencies, $F = 90$ and $F = 110$. Upstream of the step the boundary layer thickness increases due to the adverse pressure gradient built by the step and TS waves undergo large exponential growth. Immediately after the step edge, the boundary layer presents a large curvature distortion as a combined effect of two quasi-simultaneous but opposite pressure gradients. At this region the mean shear profile exhibits two different maxima and the TS waves manifest a new lobe at a near wall location where no recirculation region is observed from DNS. Further downstream the disturbance depicts a complex growth behavior characterized by highly distorted TS shape functions at locations where the meanflow has already recovered to clean case conditions. Furthermore, the $|\hat{u}|$ and $|\hat{v}|$ maxima of the fundamental mode present different amplification trends, pointing towards non-modal growth mechanisms active in these regions. Examination of the DNS perturbation flowfield in this area exhibits the tilting direction of disturbances with respect to the mean shear to be closely related to a change of sign in the production term. These findings indicate that the Orr-mechanism could play a role in the non-modal growth of disturbances after the step. Finally, immediately after the step corner, a vortical structure is observed in the perturbation field counterrotating the incoming TS waves. This near-wall feature emerges in regions of high mean shear, with no recirculating flow, where both $|\hat{u}|$ and $|\hat{v}|$ maxima undergo a steep decay. The mechanisms giving rise to this structure remain unclear.

Future numerical and experimental works should investigate the effect that changing the step height and incoming TS wave amplitude has on the growth mechanisms dominant in the vicinity of the step. This could help understand which parameters result more detrimental for laminar-turbulent transition with FFS.

REFERENCES

Åkervik, E, Ehrenstein, U, Gallaire, F & Henningson, DS 2008 Global two-dimensional stability measures of the flat plate boundary-layer flow. *European Journal of Mechanics-B/Fluids* **27** (5), 501–513.

Casacuberta, J, Hickel, S & Kotsonis, M 2021 Mechanisms of interaction between stationary crossflow instabilities and forward-facing steps. In *AIAA Scitech 2021 Forum*, p. 0854.

Costantini, M 2016 Experimental analysis of geometric, pressure gradient and surface temperature effects on boundary-layer transition in compressible high reynolds number flows. PhD thesis, Rheinisch-Westfälische Technische Hochschule Aachen.

Crouch, JD & Kosorygin, VS 2020 Surface step effects on boundary-layer transition dominated by tollmien–schlichting instability. *AIAA Journal* **58** (7), 2943–2950.

Crouch, JD, Kosorygin, VS & Ng, LL 2006 Modeling the effects of steps on boundary-layer transition. In *IUTAM Symposium on Laminar-Turbulent Transition*, pp. 37–44. Springer.

Drake, A, Bender, A, Korntheuer, A, Westphal, R, Rohe, W, Dale, G, McKeon, B & Geraschchenko, S 2010 Step excrescence effects for manufacturing tolerances on laminar flow wings. In *48th AIAA Aerospace Sciences Meeting Including the New Horizons Forum and Aerospace Exposition*, p. 375.

Edelmann, CA 2014 Influence of forward-facing steps on laminar-turbulent transition. PhD thesis, University of Stuttgart.

Eppink, JL 2020 Mechanisms of stationary cross-flow instability growth and breakdown induced by forward-facing steps. *Journal of Fluid Mechanics* **897**, A15.

Fischer, PF, Lottes, JW & Kerkemeier, SG 2008 Nek5000 web page. `http://nek5000.mcs.anl.gov`.

Jin, V, Symon, S & Illingworth, SJ 2021 Energy transfer mechanisms and resolvent analysis in the cylinder wake. *Physical Review Fluids* **6** (2), 024702.

Lin, N, Reed, HL & Saric, WS 1992 Effect of leading-edge geometry on boundary-layer receptivity to freestream sound. In *Instability, Transition, and Turbulence*, pp. 421–440. Springer.

Perraud, J, Arnal, D, Seraudie, A & Tran, D 2004 Laminar-turbulent transition on aerodynamic surfaces with imperfections. *NATO Research and Technology Organisation Applied Vehicle Technology Panel 111 Symposium* **13**.

Rius-Vidales, AF & Kotsonis, M 2021 Impact of a forward-facing step on the development of crossflow instability. *Journal of Fluid Mechanics* **924**, A34.

Tropea, C, Yarin, AL, Foss, JF *et al.* 2007 *Springer handbook of experimental fluid mechanics*, , vol. 1. Springer.

Wang, YX & Gaster, M 2005 Effect of surface steps on boundary layer transition. *Experiments in Fluids* **39** (4), 679–686.